Engineered Science
DOI: https://dx.doi.org/10.30919/es1856

Investigating the Fracture Treatment Mechanism of *Dipsacus asper* Based on Network Pharmacology, Molecular Docking and Molecular Dynamics Simulation

Zhizhong Yang,[1,#] Dongmei Guo,[1,#] Yanmei Fu,[1] Luming Qi,[2] Tiantian Zhu,[1] Xiaohui Ma,[1,*] Aili Zhang[1,*] and Kui Zhao[1,*]

Abstract

This study investigated the active components of *Dipsacus asper* (DA)in promoting fracture healing and their molecular mechanisms. The *DA* chemical constituents were sourced from the TCMSP and HERB databases. Six key components were identified based on the top six Degree values, including Japonine, ursolic acid, and Sweroside aglycone, among which exhibited the binding energy with NTRK1 (-6.69 kcal/mol), MMP9 (-6.62 kcal/mol), and CA2 (-5.86 kcal/mol). KEGG enrichment analysis revealed that *Dipsacus asper* primarily modulates the MAPK signaling pathway (promoting cell proliferation), the AGE-RAGE pathway (regulating the bone microenvironment), and ECM remodeling pathways (such as pathways in cancer). Molecular dynamics simulations demonstrated that all complexes reached stable RMSD values within 2-3 ns (fluctuations < 0.1-1 nm). A decrease in Rg values indicated more compact structures, and the CA2-Sweroside aglycone complex maintained an average of one hydrogen bond, confirming stable binding.By modulating multiple pathways such as MAPK and AGE-RAGE, it facilitates osteogenic differentiation, suppresses inflammation, and accelerates bone matrix remodeling. After MS/MS verification, the presence of Japonine in the medicinal extract was ruled out. The integrative strategy of "component-target-pathway" established in this research introduces a fresh framework for explaining how Chinese medicine works.

Keywords: Dipsacus asper; Fracture healing; Network pharmacology; Molecular docking; Molecular dynamics simulation.
Received: 24 September 2025; Revised: 30 October 2025; Accepted: 05 November 2025
Article Type: Research article.

1. Introduction

Fractures are a significant cause of disability. Due to the complexity of the fracture healing process, approximately 10% of patients experiencing delayed healing or nonunion, even with strict adherence to standard reduction and fixation protocols.[1,2] Nonunion often requires secondary surgery, and postoperative functional recovery presents significant challenges, severely affecting the patient's quality of life and work capacity. Therefore, exploring effective approaches to promote fracture healing has always been one of the central objectives in trauma and orthopedic research.[3-5] Currently, there are limited options for biological agents that directly promote fracture healing. Although Bone Morphogenetic Protein-2 (BMP-2) has received approval for clinical application in the United States,[6] it carries the risk of heterotopic ossification. Studies have also shown that BMP-2 may increase the rate of postoperative failure of internal fixation, with some patients even experiencing life-threatening complications.[7,8] Furthermore, the localized high-dose application of BMP-2 carries a potential risk of inducing malignant tumors.

DIPSACI Radix is the dried root of *Dipsacus asper* Wall. ex Henry (Fam. Dipsacaceae). It was originally named "Xuduan" in the Shennong Ben Cao Jing (Divine Farmer's Materia Medica Classic), and continues to be referred to by this name. It is an herb commonly found in traditional Chinese medicine.[9] Studies have shown that *DA* possesses properties such as bone protection and improvement of osteoporosis, demonstrating significant effects in the intervention and treatment of osteoporotic fractures.[10-12] It is one of the most commonly used Chinese medicines for treating such fractures. Although numerous studies have explored the role of *Dipsacus asper* in promoting fracture healing, its mechanism of action remains unclear. Elucidating this mechanism could

[1]*Yunnan Key Laboratory of Southern Medicinal Utilization, Yunnan Key Laboratory of Chinese Medicine Processing, Key Laboratory of Yunnan Provincial Department of Education for Processing Research on Characteristic Prepared Drug in Pieces, Key Laboratory of Yunnan Provincial Department of Education on Substance Benchmark Research of Ethnic Medicines, Yunnan University of Chinese Medicine, 1076 Yuhua Road, Kunming, Yunnan, 650500, China*

provide research insights for the clinical promotion of DA in fracture treatment and the development of new drugs.

Network pharmacology is crucial in systems biology, connecting traditional Chinese medicine concepts with modern pharmacological studies. It allows scientists to create layered networks to systematically explain the mechanisms of action of Chinese medicine, which involve multiple components and targets.[13-15] As a mature theoretical tool, molecular docking technology has become a valuable aid in the field of drug design. It facilitates the prediction of interactions at the molecular level, especially involving small molecule ligands and biological macromolecules, and enables the estimation of binding free energy.[16] In addition, molecular dynamics simulation is a method that models experimental conditions on a molecular scale, providing a visual depiction of experimental phenomena. It helps to understand patterns and mechanisms, ultimately driving research in pharmacy, chemistry, biology, and materials science toward pathways that more cost-effective, efficient, and predictive. Currently, numerous studies focus on investigating the mechanisms of drug actions on diseases by integrating network pharmacology, molecular docking, and molecular dynamics simulations.[17-19]

To better understand the mechanism of *DA* in intervening in fracture healing, this study employs network pharmacology, molecular docking, and molecular dynamics simulations to systematically investigate the related mechanisms at the molecular level, focusing on chemical components, target interactions, and signaling pathways. The aim is to establish a theoretical foundation for further clarifying the pharmacological mechanism of *DA*.

2. Materials and methods

2.1 Screening of related compounds and targets of *DA*

Data on the chemical makeup of *DA* was collected using the Traditional Chinese Medicine Systems Pharmacology Database and Analysis Platform (TCMSP) (https://old.tcmsp-e.com/tcmsp.php) combined with a literature review. The screening criteria for effective active ingredients included an oral bioavailability of at least 30% and a drug-likeness score of 0.18 or higher.[20] The targets for these active ingredients were then identified using the TCMSP database.

The High-throughput Experiment- and Reference-guided Database of Traditional Chinese Medicine (HERB) (http://herb.ac.cn/) was also used to obtain chemical components. The molecular structures of the compounds sourced from the HERB database were individually retrieved one by one via the PubChem database (https://pubchem.ncbi.nlm.nih.gov) and saved in 3D.sdf format.[21] The structures of the acquired compounds were imported into the SwissADME platform (http://www.swissadme.ch/).[22] The criteria for potential core compounds were set as follows: (1) Gastrointestinal absorption (GI absorption) must be "High", indicating the component possesses good oral bioavailability and can be absorbed; (2) Results from five drug-likeness rules (Lipinski, Ghose, Veber, Egan, Muegge) must include two or more "Yes" outcomes. Subsequently, compounds excluded based on the screening criteria were re-evaluated through literature verification. Compounds with notable pharmacological effects pertinent to the research were still included, ultimately obtaining potential compounds related to the research topic. Using the SwissTargetPrediction platform (http://www.swisstargetprediction.ch/), the targets for these potential compounds were predicted based on their structural similarities in both 2D and 3D to known compounds.[23] Target proteins with a probability score greater than zero were chosen. Furthermore, targets of active compounds that were known but not predicted by the platform were supplemented based on published literature reports on drug-related components.

2.2 Screening of fracture-related targets

To ensure data accuracy and comprehensiveness, "fracture" was used as a keyword to search the Online Mendelian Inheritance in Man (OMIM) database (http://www.omim.org) and the GeneCards database (https://www.genecards.org) to obtain core fracture-related targets.[24-26] The OMIM and GeneCards databases are literature-based, with each database having its own advantages and complementing one another. Targets obtained from the above databases were merged after removing duplicates. Additionally, known targets of active compounds that were not predicted were supplemented based on literature reports. The UniProt protein database (https://www.uniprot.org) served to convert disease targets and drug component targets into official gene symbols.[27] Subsequently, the two sets were mapped to identify potential targets of Dipsacus asperoides for promoting fracture healing.

2.3 Building the PPI network for dipsacus asper compound-fracture target

The study of Protein-protein interaction (PPI) networks focuses on the connections between compounds and proteins linked to diseases, considering biochemistry, signal transduction, and genetic networks. To clarify the function of target proteins on a systems level, the aforementioned targets were entered into the STRING 12.0 database (https://string-db.org), PPI network relationships were obtained by selecting

[2]*School of Health Preservation and Rehabilitation, Chengdu University of Traditional Chinese Medicine, Chengdu, Sichuan, 611137, China*
[#]*These authors have contributed equally to this work*
[*]*Email:* maxiaohui1988@126.com (Xiaohui Ma),
Zhangailibb@126.com (Aili Zhang),
zhaok06@ynucm.edu.cn (Kui Zhao)

"Homo Sapiens" as the species and setting the confidence score for target associations to 0.40.[28] The data were subsequently loaded into CytoScape 3.7.1 software. Using the cytoHubba plugin within CytoScape 3.7.1, the MCC algorithm was applied to pinpoint hub proteins, enhancing sensitivity and specificity. Here, the biological network G = (V, E) is considered to be undirected, with V representing the nodes and E representing the edges.[29,30] Alternatively, the network can be represented as G = (V(G), E(G)), where V(G) represents the nodes in network G and E(G) represents the edges in network G. The cardinality of a set S, denoted as |S|, refers to the number of elements within the set. MCC is based on the notion that vital proteins usually group in yeast protein-protein interaction networks. The definition of a node v in MCC is Eq. (1):

$$MCC(v) = \sum_{C \in S(v)} (|C|-1)! \quad (1)$$

2.4 GO functional enrichment and KEGG pathway enrichment analysis of dipsacus asper ingredients and fracture-related targets

The Metascape platform was used for bioinformatic enrichment analysis of the target genes, incorporating Gene Ontology (GO) analysis for biological processes (BP), molecular functions (MF), and cellular components (CC), along with KEGG pathway analysis.[31] The results of each analysis were sorted in ascending order based on P-value, using a screening threshold of $P < 0.05$. The 20 most significantly enriched GO terms and KEGG pathways meeting the criteria were selected, and the results were subjected to visualization analysis and processing.

2.5 Molecular docking evaluation

Select targets with high degree values from the analyzed network diagram of *DA* ingredients and fracture-related targets. Access the RCSB database (http://www.rcsb.org/pdb) to download the 3D crystal structures of the target proteins and keep them in PDB format.[32] Convert the 3D chemical structures of the candidate compounds into PDB format files with Open Babel 3.1.1 (http://openbabel.org/wiki/Main_Page).[33] Employ AutoDockTools 1.5.7 (http://autodock.scripps.edu/resources/tools) to remove water molecules, introduce hydrogen atoms, calculate Gasteiger charges, and assign AD4 type rigid properties, then save the files in PDBQT format.[34] Perform molecular docking with AutoDock 4.2.6, and calculate the binding energy to assess the binding activity of small molecules with proteins. In general, a docking binding energy under -5.0 kJ/mol is regarded as a marker of good binding interaction. Finally, use the Protein-Ligand Interaction Profiler (PLIP) platform (https://plip-tool.biotec.tu-dresden.de/plip-web/plip/index) to identify non-covalent interactions between biomacromolecules and their ligands, and visualize the results using PyMOL 2.4.0 software.[35,36]

2.6 Simulation of molecular dynamics and calculation of binding free energy

First, use Gaussian 16 (https://gaussian.com/gaussian16/) and GaussView 6 software (https://gaussian.com/gaussview6/) to perform structural optimization of the ligand. After importing the ligand structure in mol2 format into GaussView 6, select "Optimization" as the task type, choose "Ground State" for the molecular state, select DFT (Density Functional Theory) as the calculation method, set the spin multiplicity to "Default Spin," choose B3LYP as the functional, select the IEF PCM solvent model, and set the solvent to water. Once the molecular structure optimization is complete, use Gaussian 16 to convert the generated chk file to an fch file. Then, import the file into Multiwfn (http://sobereva.com/multiwfn/) to calculate the RESP charge of the ligand.

The Restrained Electrostatic Potential (RESP) model is currently the most suitable atomic charge calculation method for molecular dynamics simulations. The RESP model addresses three major shortcomings of traditional electrostatic potential (ESP)-fitted atomic charges: in conventional ESP fitting, buried atoms (such as sp^3 carbons) exhibit numerically unstable charge values due to their distance from sampling points. To mitigate this, RESP introduces a hyperbolic penalty function (Eq. (2)) in the objective function[37].

$$\chi^2_{restr} = a \sum_j \left(\sqrt{q_j^2 + b^2} - b \right) \backslash tag9 \quad (2)$$

where the parameter a controls the restraint strength (recommended values: a = 0.0005 for weak restraints, a = 0.001 for strong restraints), and b = 0.1 adjusts the curvature of the hyperbolic function. The derivative of this function approaches a constant $a \cdot \mathrm{sign}(q_j)$ when $|q_j| \gg b$, thereby avoiding excessive penalties on large charges, thereby prioritizing the suppression of anomalous charges in buried atoms without compromising the charge accuracy of polar atoms. Compared to harmonic restraints, hyperbolic restraints effectively preserve deterministically large charges (*e.g.*, on oxygen and nitrogen atoms) while significantly reducing charge magnitudes in nonpolar regions (*e.g.*, methyl carbon charges decrease from ±0.4e to ±0.2e).

For rapidly rotating symmetric groups (such as methyl hydrogens), RESP employs a two-stage optimization strategy: Stage 1 (wk.fr): All atoms are freely fitted under weak restraints to preserve charge details in polar regions (*e.g.*, carboxyl oxygen charge errors < 0.02e). Stage 2 (st.eq): The charges of polar atoms are frozen, while strong restraints are applied to symmetric groups for refitting, ensuring equivalent charges for methyl hydrogens and further convergence of carbon charges (Table IX shows a 30% reduction in errors). This strategy decouples local symmetry handling from global ESP fitting, maintaining dipole moment accuracy while addressing the degradation of ESP quality caused by direct constraints or post-averaging methods.

RESP employs the 6-31G* basis set to compute quantum mechanical ESP. Although this may lead to overpolarization

in the gas phase, it effectively balances the TIP3P water model with intramolecular polarization effects by generating grids at 1.4 to 2.0 times the van der Waals radius (density: 1 point/Å^2). Combined with the RESP2 extended model (introducing δ=0.6 to weight aqueous and gas phases), the charge transferability across molecules is improved. For example, charge differences for the same functional group in different molecules are reduced from ±0.15e to ±0.05e. The matrix equation for solving is Eq. (3) [37]:

$$Aq=B \text{ where } A_{jk}=\sum_i \frac{1}{r_{ij}r_{ik}}+\frac{\partial \chi^2_{restr}}{\partial q_j} \quad (3)$$

It provides the exact least-squares solution directly, avoiding initial guess bias in iterative methods and ensuring numerical stability of the charges.

After completing the RESP charge calculation, import the generated chg file into sobtop 1.0 (dev5) software (http://sobereva.com/soft/Sobtop/) to generate the ligand topology file required for molecular dynamics simulations. Using GROMACS 2019.6 software,[37] molecular dynamics simulations were carried out with the AMBER99 force field.

The structural files of the protein and small molecules were imported into the software, and a triclinic box with periodic boundary conditions of 1.0 nm was constructed, followed by solvation using the TIP3P water model. The Particle Mesh Ewald (PME) method was employed to calculate long-range electrostatic interactions. An appropriate number of sodium and chloride ions were added using the gmx genion command to neutralize the system charge. Simulations were conducted under a constant temperature of 298 K and a standard atmospheric pressure of 100 kPa.

To minimize energy, the steepest descent algorithm was applied. Using gmx grompp and gmx mdrun commands, 10,000 energy minimization steps were performed, followed by equilibration in the NVT (isothermal-isochoric) and NPT (isothermal-isobaric) ensembles. Temperature and pressure were coupled with constants of 0.1 ps and 0.5 ps, respectively, and the total equilibration period was 100 ps. Following system equilibration, a 10 ns production molecular dynamics simulation was performed on the complex with a 2 fs time step, saving trajectory data every 2 ps.

Further analyses included the calculation of root mean square deviation (RMSD), root mean square fluctuation (RMSF), protein radius of gyration, hydrogen bonds, and solvent accessible surface area (SASA) utilizing the gmx rms, gmx rmsf, gmx gyrate, and gmx hbond commands, respectively. The results were depicted using QTgrace (https://sourceforge.net/projects/qtgrace/).

2.7 Validation by UPLC-QTOF-MS/MS

Due to the fixed processing methods adopted in the experimental operation, there will be certain deviations from those in the database. Therefore, mass spectrometry analysis of the commonly used extraction methods is required to verify the results.

Preparation of methanol extract from *DA*: Accurately weigh 0.5 g of broken powder, add 25 mL of methanol, sonicate for 30 minutes, let it stand at room temperature, shake well, filter, take the supernatant and filter it through a 0.22 μm microporous membrane to obtain the test solution.

UPLC-QTOF-MS/MS analysis: The chemical composition of *DA* were analyzed using UPLC-Q-TOF-MS/MS technology. Using ultra-high performance liquid chromatography combined with Q Exactive Orbitrap LC-MS/MS high-resolution mass spectrometer (Thermo Fisher, USA) and *Natural Product and Metabolite Profiles* database (300 thousand), qualitative analysis of chemical components in the ethanol extract of *DA* was carried out.

3. Results

3.1 Screening of active compounds

There were 16 active ingredients identified in *DA*, equally divided between the TCMSP and HERB databases. The TCMSP database yielded 31 chemical components, from which 8 active ingredients were screened using the criteria of OB at least 30% and DL at least 0.18. The HERB database provided 35 chemical components, and screening via the SwissADME platform resulted in 15 active ingredients. Among these, 7 active ingredients had already been identified in the TCMSP screening, thus adding 8 new active ingredients. The active ingredients of *DA* are detailed in Table 1.

3.2 Acquisition of intervention targets for fracture healing

The structural sdf files of the 8 newly added active ingredients of *DA* sourced from the HERB database, were uploaded to SwissTargetPrediction to forecast the target proteins of the active pharmaceutical ingredients. A total of 395 drug targets were identified after merging with the drug targets from the TCMSP database and eliminating duplicates.

From the Genecards database, 6,749 fracture-related targets were identified. By selecting targets with a relevance score of ≥5.509503365, 231 potential fracture-related disease targets were determined. A total of 232 disease targets were identified after integrating with targets from the OMIM database. The overlap between the 395 targets of *DA* and the 232 fracture-related targets yielded 27 common targets. In Fig.1(A), the results were visualized in a Venn diagram created with the Venny 2.1.0 platform (https://bioinfogp.cnb.csic.es/tools/venny/).

3.3 Building the PPI network

In Fig.1(B), the 27 intersecting targets were entered intothe STRING 12.0 database to acquire PPI network information, and the target protein PPI network was reconstructed using Cytoscape 3.7.1. After obtaining the PPI network, the

Table 1: The active ingredients in *Dipsacus asper*.

Mol ID/Ingredient id	Molecule Name	InChIKey
MOL003152 (HBIN027522)	Gentisin	XOXYHGOIRWABTC-UHFFFAOYSA-N
MOL000358	beta-sitosterol	KZJWDPNRJALLNS-VJSFXXLFSA-N
MOL000359 (HBIN044158)	sitosterol	KZJWDPNRJALLNS-ZFVHJZABSA-N
MOL009312 (HBIN024871)	(E,E)-3,5-Di-O-caffeoylquinic acid	KRZBCHWVBQOTNZ-ZURXXRFOSA-N
MOL009317 (HBIN019981)	Cauloside A_qt	CPPAMFUQVBDPTG-XDGYBBFPSA-N
MOL008188 (HBIN031441)	Japonine	XTBMLWZKNWXUHV-UHFFFAOYSA-N
MOL009322 (HBIN045208)	Sylvestroside III	MALYQXLMMWQXME-YWSLBQKTSA-N
MOL009323 (HBIN045209)	Sylvestroside III qt	HPPQDJKDCBOQBR-HORHJMKNSA-N
HBIN019622 (MOL009314)	Cantleyine	MJGLQDXKEOEIFB-LDWIPMOCSA-N
HBIN034784 (MOL009313)	Mesitol	BPRYUXCVCCNUFE-UHFFFAOYSA-N
HBIN039127 (MOL000661)	PENTACOSANOIC ACID	MWMPEAHGUXCSMY-UHFFFAOYSA-N
HBIN040358 (MOL001714)	podophyllotoxin	YJGVMLPVUAXIQN-XVVDYKMHSA-N
HBIN045176 (MOL000651)	Sweroside aglycone	HBAKFDGYROBYSH-BKPPORCPSA-N
HBIN046166	thalicarpine	ZCTJIMXXSXQXRI-KYJUHHDHSA-N
HBIN047613(MOL000511)	ursolic acid	WCGUUGGRBIKTOS-GPOJBZKASA-N
HBIN047793(MOL000652)	Venoterpine	IOIGOIPHPUCFOB-HZGVNTEJSA-N

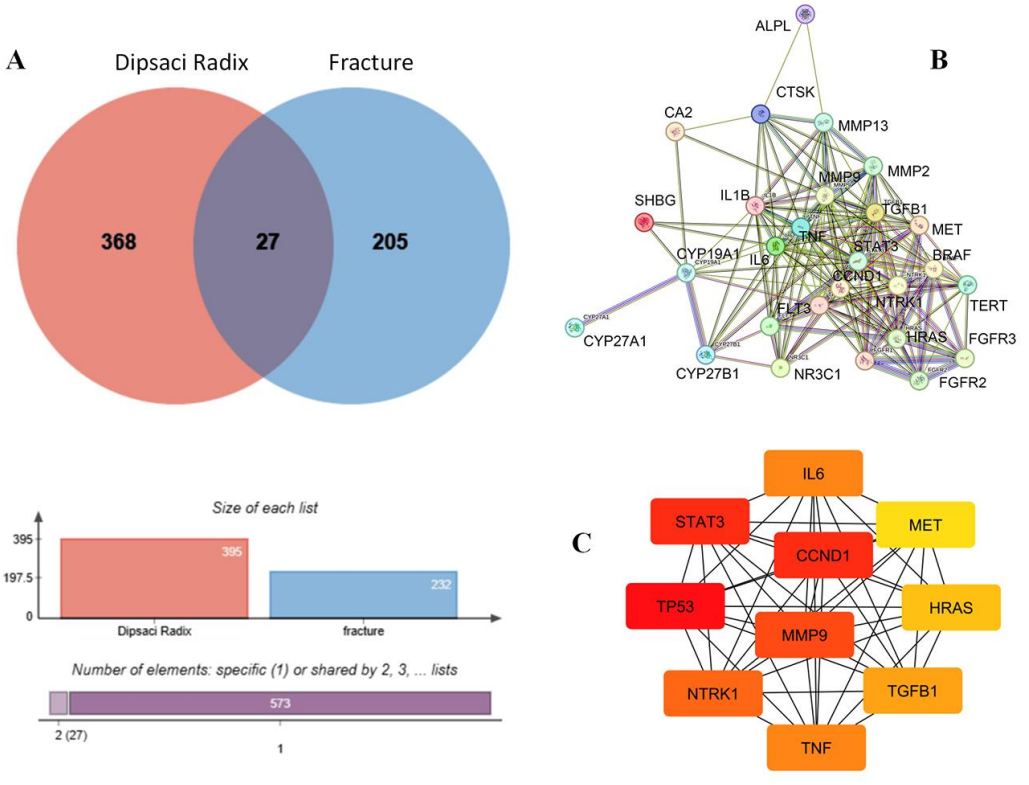

Fig. 1: Screening of target. (A) *DA* targets and fracture healing targets; (B) PPI network of target protein; (C) Core targets.

cytoHubba plugin in Cytoscape was used to analyze the data with the MCC algorithm, and the top ten targets were defined as core targets.They are presented in Fig. 1(C).

3.4 Construction of the fracture-active ingredients of *DA*-targets network

The active compounds of *DA* and their targets were loaded into Cytoscape 3.7.1 for network visualization, and nodes representing active compounds with a degree of 0 were excluded. In Fig. 2, the central node represents fractures, circular nodes represent intersecting targets, square nodes signify active drug ingredients, and the edges between nodes indicate the interaction relationships between ingredients and targets. The predicted targets were analyzed using their Degree values, and the six targets with the highest Degree values are listed in Table 2. In the diagram, larger node areas correspond to higher Degree values, indicating stronger relationships with other targets and suggesting that the active ingredient plays

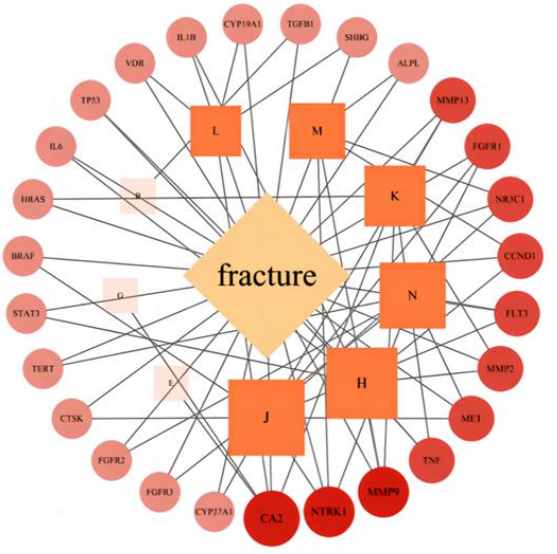

Fig. 2: Disease-active ingredients-targets network.

Table 2: The top 6 active ingredients of *Dipsacus asper.*

No.	Ingredients	Degree
J:MOL008188	Japonine	9
H:MOL000511	ursolic acid	8
N:HBIN046166	thalicarpine	7
K:MOL009322	Sylvestroside II	6
M:MOL001714	podophyllotoxin	5
G:MOL000651	Sweroside aglycone	1

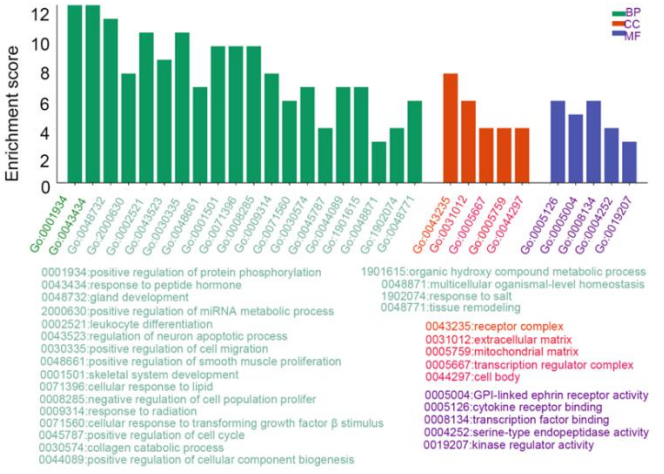

Fig. 3: GO enrichment analysis.

a key role in the entire network. According to Degree value, the six leading active ingredients are Japonine, Ursolic acid, Thalicarpine, Sylvestroside III, Podophyllotoxin, and Sweroside aglycone.

3.5 GO functional enrichment and KEGG pathway enrichment

The Metascape platform was used for bioinformatic enrichment analysis of the intersecting targets, and the results were visualized via the bioinformatics platform (https://www.bioinformatics.com.cn/). The analysis of GO functional enrichment identified 30 significant GO terms ($P < 0.05$), including 20 biological process (BP) terms, 5 cellular component (CC) terms, and 5 molecular function (MF) terms, accounting for 66.7%, 16.7%, and 16.7% respectively (Fig. 3). Fig. 4 shows the outcomes of the KEGG pathway analysis, screening 8 significantly enriched signaling pathways ($P < 0.05$). Among these pathways are the cancer pathways, MAPK signaling pathway, proteoglycans in cancer, and the AGE-RAGE signaling pathway related to diabetic complications.

3.6 Molecular docking

According to the literature, a docking energy below -4.25 kcal/mol shows binding activity between the ligand and target, while a docking energy below -5.0 kcal/mol indicates relatively strong binding, and a docking energy below -7.0 kcal/mol denotes very strong binding.[38,39] The molecular docking results obtained from AutoDockTools 1.5.7 (Table 3 and Fig. 5) show that the binding energy between Japonine, a major active compound in Dipsacus asperoides, and NTRK1 is -6.69 kcal/mol; The binding energy of ursolic acid with MMP9 is -6.62 kcal/mol, and that of Sweroside aglycone with CA2 is -5.86 kcal/mol. All these docking energies are < -5.0 kcal/mol. Therefore, Japonine, ursolic acid, and Sweroside aglycone exhibit strong binding activity with the core target

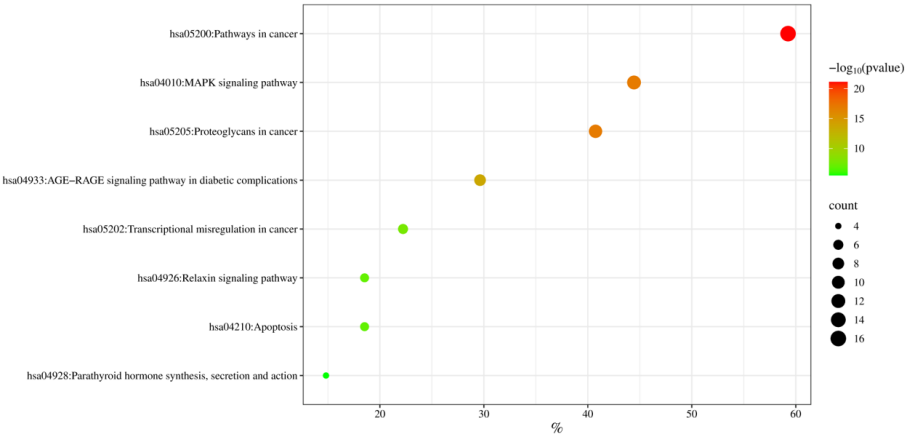

Fig. 4: KEGG enrichment analysis.

Table 3: Docking energy.

Receptor	Ligand number	Ligand name	Docking energy (kcal/mol)
NTRK1	J:MOL008188	Japonine	-6.69
MMP9	H:MOL000511	ursolic acid	-6.62
CA2	G:MOL000651	Sweroside aglycone	-5.86

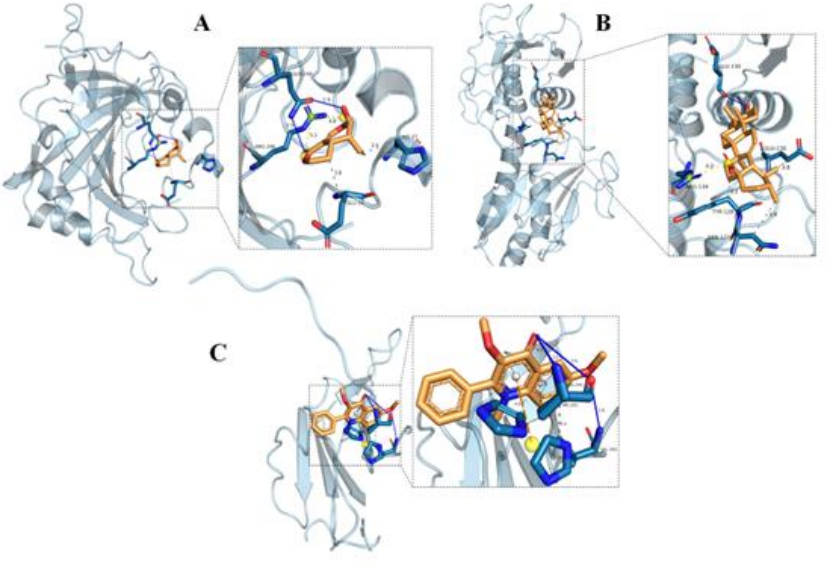

Fig. 5: Molecular docking. (A) CA2_Sweroside aglycone; (B) MMP9_ursolic acid; (C) NTRK1_Japonine.

macromolecular receptors NTRK1, MMP9, and CA2. These docking results provide valuable data support for the future experimental screening and design of related Chinese medicines and their active components.

3.7 Results of molecular dynamics simulation

According to relevant literature reports and molecular docking results, NTRK1, MMP9, and CA2 are predicted to be important targets of *DA* in the treatment of fractures. This study further employed molecular dynamics simulations to examine the binding stability of the active components of *DA* with the predicted targets. The results of the root mean square deviation (RMSD), root mean square fluctuation (RMSF), radius of gyration (Rg), hydrogen bonds (hbonds), and

solvent-accessibility surface area (SASA) between the active components of *DA* and the predicted targets on the proteins were obtained and visualized using OTgrace.

As shown in Fig. S1(C), during the initial stage of the molecular dynamics simulation (0-2 ns), the RMSD values between NTRK1 and Japonine exhibited significant changes. After 2 ns, the fluctuations in the RMSD curve decreased and stabilized, with a variation range of less than 1 nm, indicating good stability and equilibrium in the binding mode of this system. In Fig. S1(B), between 0-3 ns, the RMSD values between MMP9 and ursolic acid showed considerable variations. After 3 ns, the fluctuations in the RMSD curve reduced and stabilized, with a variation range of less than 0.1 nm, demonstrating high stability and equilibrium in the binding mode of this system. As illustrated in Fig. S1(A), during the initial stage of the molecular dynamics simulation (0-2 ns), the RMSD values between CA2 and sweroside underwent significant changes. After 2 ns, the fluctuations in the RMSD curve decreased and stabilized, with a variation range of less than 0.1 nm, suggesting good stability and equilibrium in the binding mode of this system.

To investigate the stability of specific parts of the complex, root mean square fluctuation (RMSF) analysis was conducted. Higher RMSF values suggest greater flexibility and lower stability in the corresponding region. Fig. S2 shows that the head and tail regions of Japonine exhibit relatively high RMSF values, which may be attributed to the presence of tightly coiled structures like α-helices and β-sheets. Conversely, lower RMSF values might suggest that corresponding structures in the complex have been lost.[40]

Analysis of the radius of gyration (Rg) was performed to understand the overall compactness of the protein structure during the simulation. An increase in Rg values typically indicates that the protein structure becomes looser or unfolds, while stable Rg values suggest that the protein maintains its overall structural compactness.

As shown in Fig. S3(A), the Rg values of the NTRK1-Japonine complex remained below 2 nm and exhibited a continuous decreasing trend throughout the simulation, indicating that the protein maintained structural compactness and a tightly packed molecular conformation. In Fig. S3(B), the Rg values of the MMP9-ursolic acid complex were higher than 2 nm and showed an increasing trend, suggesting that the complex possesses structural flexibility and expansibility, potentially containing disordered regions or undergoing partial unfolding. In Fig. S3(C), the gradually decreasing Rg values of the CA2-sweroside complex during the simulation indicate that the complex structure progressively stabilized and adopted a more tightly packed molecular arrangement.

Hydrogen bond analysis was performed to comprehend their role in molecular binding. Hydrogen bonds enhance binding affinity, and typically, a higher number of hydrogen bonds suggests stronger binding. However, the findings showed that the protein-ligand hydrogen bonds were fewer than those found in the earlier molecular docking research. This discrepancy may be attributed to the following reasons:

Molecular docking identifies the lowest energy conformation of the ligand-receptor complex through energy optimization. When calculating hydrogen bonds, it considers only a single static structure and employs relaxed geometric criteria, which may include transient or unstable hydrogen bonds. In contrast, GROMACS adopts strict geometric standards (default criteria: D–A distance ≤ 0.35 nm (3.5 Å), D–H–A angle ≤ 30°) and accounts for standard angle fluctuations, leading to the exclusion of some hydrogen bonds from statistical results. Molecular docking programs (such as AutoDock) compute hydrogen bonds based on a single energy-minimized static structure, whereas molecular dynamics simulations quantify hydrogen bonds that persist, with high occupancy (*e.g.*, >90% of the simulation time), thereby filtering out transient interactions. Furthermore molecular dynamics simulations incorporate explicit water molecules, which can form hydrogen bonds with the ligand or receptor and compete for binding sites. Solvent molecules may shield interactions between solutes through hydrogen bonding, resulting in the replacement of some ligand-receptor hydrogen bonds. In contrast, molecular docking typically uses implicit solvent models (*e.g.*, GB/SA), which cannot simulate the competitive effects of water molecules. Therefore, molecular docking tends to overestimate the number of hydrogen bonds, while GROMACS-based molecular dynamics simulations retain only stable hydrogen bonds, leading to a reduction in the statistically reported number (Fig. S4).

The solvent accessible surface area (SASA) plot illustrates the protein's surface area that is exposed to the solvent during the simulation. An increase in SASA values indicates greater exposure of hydrophobic residues to the solvent, which may be related to protein flexibility or structural changes.

In Fig. S5(A), some regions exhibit SASA values smaller than 50 Å^2, indicating that these areas are highly compact with minimal exposure to the solvent, possibly located in the protein core or engaged in tight interactions with other molecules. In Fig. S5(B), SASA values greater than 200 Å^2 suggest significant solvent exposure, which may correspond to molecular surface regions, functional areas, or disordered regions with high dynamics. In Fig. S5(C), SASA values between 50 and 200 Å^2 represent moderately exposed regions, likely situated on the molecular surface or exhibiting a certain degree of flexibility.

3.8 UPLC-QTOF-MS/MS Identification

The total ion current diagram in positive and negative ion modes were shown in Fig. 6. From the chromatogram, it can be found that there are similar parts in different modes of the continuous extract, but there are more differences. These provide a lot of objective evidence for our analysis.

The *.RAW* data obtained through different ion modes were combined with the existing components of the reported medicinal materials in the database to obtain high-scoring results and verify them. The following typical compounds

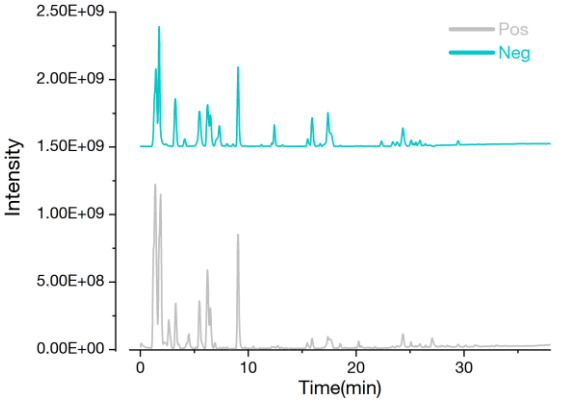

Fig. 6: The total ion current diagram in positive and negative ion modes.

Table 4: UPLC-QTOF-MS/MS Identification Results of Compounds in *Dipsacus asper*.

ID	Chemical Names	Molecular formula	Complex ion	Measured value (m/z)	Secondary mass (m/z)
1	Ursolic acid	C30H48O3	[M-H2O+H]+1	439.36	439, 393, 249, 203, 191, 107, 121, 95
2	Isochlorogenic acid A(E,E)-3,5-Di-O-caffeoylquinic acid)	C25H24O12	[M+H]+1	517.13	499, 337, 319, 163, 135, 117, 107, 89, 79
3	Gallic acid	C7H6O5	[M-H]-1	169.01	169, 152, 124, 78 50
4	D-Trehalose	C12H22O11	[M-H]-1	341.10	341, 281, 179, 135, 119, 89, 71
5	Sylvestroside I	C33H48O19	[M+H]+1	749..28	551, 533, 389, 323, 215, 193, 179, 161,. 153, 127, 111, 81
6	Hederagenin + O-Hex	C36H58O9	[M+FA-H]-1	679.41	679, 633, 471, 314, 207, 77
7	Hederagenin + O-Acetyl Hex	C38H60O10	[M+FA-H]-1	721.42	721, 591, 429, 314, 207, 77
8	3-Hydroxybenzyl alcohol	C7H8O2	[M+H]+1	124.14	124, 107, 93
9	trans-Cinnamaldehyde	C9H8O	[M+H]+1	133.06	133, 116, 105, 95, 79, 70, 55
10	Loganin	C17H26O10	[M+FA-H]-1	435.15	435, 357, 227, 213, 127, 113, 101, 89, 71, 68, 59
11	Caffeic acid	C9H8O4	[M-H]-1	179.04	179, 135, 116, 105, 95, 89, 71
12	Catechin	C15H14O6	[M+H]+1	291.07	291, 259, 86, 69
13	Loganic acid	C16H24O10	[M-H]-1	375.129	375, 213, 169, 151, 119, 113, 89, 69, 59
14	Azelaic acid	C9H16O4	[M-H]-1	187.10	187, 125, 111, 97
15	Sweroside	C16H22O9	[M+Na]+1	381.11	381, 279, 255, 219, 149, 95, 56
16	Podophyllotoxin	C22H22O8	[M+H]+1	415.14	415, 397, 313, 282, 239, 229,. 196, 173, 151, 143, 115
17	Geniposide	C17H24O10	[M+FA-H]-1	433.14	433, 387, 225, 127, 123, 101, 69
18	6'-O-beta-D-Apiofuranosylsweroside	C21H30O13	[M-H]-1	489.16	489, 370, 248, 191, 177, 151, 149, 131,125, 89, 81, 59
19	Dihydroxycoumarin	C9H6O4	[M-H]-1	177.02	177, 149, 133, 105, 89, 81, 71

ID	Chemical Names	Molecular formula	Complex ion	Measured value (m/z)	Secondary mass (m/z)
20	Caffeoyl quinic acid	C16H18O9	[M-H]-1	353.09	353, 191, 179, 161, 135, 127, 111, 85, 71, 59
21	4'-Demethylepi-podophyllotoxin	C21H20O8	[M+H]+1	401.12	401, 383, 351, 299, 268, 225, 182, 151, 143, 115
22	(1R,3R,4S,5R)-3-[(E)-3-(3,4-dihydroxyphenyl)prop-2-enoyl]oxy-1,5-dihydroxy-4-[(E)-3-(3-hydroxy-4-methoxyphenyl)prop-2-enoyl]oxycyclohexane-1-carboxylic acid	C26H26O12	[M-H]-1	529.14	529, 367, 353, 191, 179, 173, 161, 133, 93, 85, 67
23	Cynarin	C25H24O12	[M+Na]+1	539.12	539, 377, 359, 215, 197, 163, 145, 135, 97, 79
24	Ritalinic acid	C13H17NO2	[M+H]+1	220.13	220, 150, 134, 119, 87
25	Asperosaponin VI	C47H76O18	[M-H]-1	927.51	603, 471, 425
26	Thalicarpine (Thaliblastine)	C41H48N2O8	[M+H]+1	697.34	697, 666, 488, 457, 427, 326, 297, 206, 189
27	Ferulic acid	C10H10O4	[M+H]+1	195.06	176, 152, 144, 116, 88
28	Icariin	C33H40O15	[M+Na]+1	669.23	669, 537, 391, 335, 107
29	Pantothenic acid	C9H17NO5	[M-H]-1	218.10	218, 188, 146, 116, 99, 88, 71

were obtained, as detailed in Table 4. Among the secondary metabolites of *DA*, the most representative components should be Triterpene saponins represented by Hederagenin, such as asperosaponin F, asperosaponin H1, and Asperosaponin VI. Although these components emerged victorious in the fracture screening of this study, as unique components of the plant, they serve as markers for tracing the origin of the medicinal material.Among them, Asperosaponin VI was detected in MS/MS assays, thus having the potential to identify the index substances of medicinal materials. Among them, the triterpene acid components, represented by Ursolic acid, were screened out and had a high binding degree with the MMP9 receptor, and were identified by MS/MS secondary mass spectrometry and database.

Another major category of active ingredients, Iridoid-like substances, includes Sweroside, Loganin, Cantleyoside. Among them, Sweroside was screened out as having high CA2 binding performance and was identified by MS/MS, demonstrating excellent credibility.

In addition to the intersection verification of the above screening results, we also identified active traditional Chinese medicine components such as Loganin, Loganic acid, Podophyllotoxin and its derivatives, Isochlorogenic acid, Gallic acid, Catechin, and Icariin. Through rational application, it can exert its unique efficacy in clinical practice. It is a pity that after multiple injections and updates to multiple mass spectrometry databases, we did not find Japonine highly bound to NTRK1 in the mass spectrometry data. This indicates the necessity of using multiple methods in combination for target disease target screening in the future.

4. Discussions

This study identified 16 active components from *DA*, among which Japonine, Ursolic acid, and Sweroside aglycone were found to regulate fracture healing through highly interconnected core targets (NTRK1, MMP9, CA2). Molecular docking verified that these three components have a stable binding with the targets (binding energy ≤ -5.00 kcal/mol), with Japonine-NTRK1 (-6.69 kcal/mol) and ursolic acid-MMP9 (-6.62 kcal/mol) demonstrating the strongest binding affinity. These targets are respectively involved in nerve growth factor signaling (NTRK1), matrix degradation and inflammation regulation (MMP9), and carbonic anhydrase II (CA2) activity, synergistically promoting osteogenic differentiation and matrix remodeling from multiple perspectives. KEGG enrichment analysis revealed that *DA* primarily intervenes in fracture healing by modulating the MAPK signaling pathway (mediating cell proliferation and inflammatory responses), the AGE-RAGE pathway (influencing oxidative stress and the bone microenvironment), and cancer-related pathways (shared pathway: modulating ECM remodeling, osteoclast development). These pathways cover the three core stages of fracture healing: the inflammatory phase (MMP9 inhibits excessive inflammation),[41] the repair phase(MAPK promotes osteoblast differentiation),[41] and the remodeling phase (CA2 facilitates osteoclast development).[42]

The component-target complexes' dynamic stability was

further supported by 10 ns molecular dynamics simulations: RMSD values stabilized after 2-3 ns (fluctuations < 0.1-1 nm), decreasing Rg values indicated more compact protein structures, maintained hydrogen bonds (*e.g.*, an average of 1 for CA2-sweroside) supported binding reliability, and low solvent accessible surface area (SASA) suggested tight regional binding with strong interactions. However, the study's reliance on database thresholds (OB/DL) might have overlooked components with low bioavailability but high activity, and did not account for in vivo metabolic transformations or synergistic effects between components. Future work should validate the regulation of NTRK1/MMP9/CA2 targets through cellular experiments and explore the specific role of the AGE-RAGE pathway in bone healing.

Ursolic acid and Sweroside were screened out and had a high binding degree with the MMP9 and CA2 receptor, and were identified by MS/MS secondary mass spectrometry and database. Although the possibility of Japonine's existence cannot be directly ruled out, the latter two, after MS/MS verification, have higher credibility. This might also be related to the extraction method. In the future, the role of Japonine in the continuous treatment of fractures can be confirmed through in vivo and in vitro experiments with standard substances.

Poly-target complexes can exert multiple therapeutic effects and present them at relatively low doses of monotherapy. When we study the precise selection of the optimal diseases and drugs, the safety issues caused by monotherapy doses are relatively reduced. In the future, it is still necessary to enhance the integration of multiple technologies with databases, apply artificial intelligence algorithms for optimization and screening, and combine internal and external verification with clinical data collection to provide more precise guidance for clinical medication.

5. Conclusion

The core active components of *DA* (such as Japonine, Ursolic acid, Sweroside, etc.) exert anti-inflammatory, osteogenic differentiation-promoting, and effects on matrix remodeling by targeting key elements such as NTRK1, MMP9, and CA2, thereby regulating MAPK, AGE-RAGE, and bone metabolism-related pathways to intervene in fracture healing. Molecular docking and dynamics simulations confirmed the stable binding between core components and targets (binding energy < -5.0 kcal/mol, stable RMSD/Rg values), providing a theoretical basis for screening active components and investigating mechanisms of *DA*. After MS/MS verification, the presence of Japonine in the medicinal extract was ruled out. The integrated "component-target-pathway" analysis framework established in this study offers a new perspective for deciphering the mechanisms of Chinese medicine compounds and the development of new pharmaceuticals.

Acknowledgments

This work was supported by the Project of Yunnan Province Basic Research Special Project - General Project (202501AT070340), "Xingdian" Talents of Yunnan - Study and Visiting Programs, and Yunnan Science and Technology Talent and Platform Program (202105AG070012).

Conflict of Interest

There is no conflict of interest.

Supporting Information

Applicable.

CRediT Statement

Zhizhong Yang, Kui Zhao and **Luming Qi:** Conceptualization, Methodology, Software, Investigation. **Zhizhong Yang, Dongmei Guo** and **Yanmei Fu:** Formal analysis, Writing - Original draft. **Tiantian Zhu** and **Aili Zhang:** Data curation, Writing, Visualization, Investigation. **Xiaohui Ma, Aili Zhang** and **Kui Zhao:** Review & Editing, Funding acquisition, Resources, Supervision.

References

[1] D. Wang, J. Wang, J. Zhou, X. Zheng, The role of adenosine receptor A2A in the regulation of macrophage exosomes and vascular endothelial cells during bone healing, *Journal of Inflammation Research*, 2021, **14**, 4001-4017, doi: 10.2147/jir.s324232.

[2] D. Wang, Y. Liu, W. Lv, W. Liang, X. Zhou, Y. Ding, J. Zhou, Repetitive brief ischemia accelerates tibial shaft fracture healing: a 5-years prospective preliminary clinical trial (PCT), *BMC Musculoskeletal Disorders*, 2021, **22**, 631, doi: 10.1186/s12891-021-04515-y.

[3] J. S. Barbosa, R. F. Mendes, F. Figueira, V. M. Gaspar, J. F. Mano, S. S. Braga, J. Rocha, F. A. Almeida Paz, Bone tissue disorders: healing through coordination chemistry, *Chemistry – A European Journal*, 2020, **26**, 15416-15437, doi: 10.1002/chem.202004529.

[4] S. B. Goodman, M. Maruyama, Inflammation, bone healing and osteonecrosis: from bedside to bench, *Journal of Inflammation Research*, 2020, **13**, 913-923, doi: 10.2147/jir.s281941.

[5] H. ElHawary, A. Baradaran, J. Abi-Rafeh, J. Vorstenbosch, L. Xu, J. I. Efanov, Bone healing and inflammation: principles of fracture and repair, *Seminars in Plastic Surgery*, 2021, **35**, 198-203, doi: 10.1055/s-0041-1732334.

[6] I. Dumic-Cule, M. Peric, L. Kucko, L. Grgurevic, M. Pecina, S. Vukicevic, Bone morphogenetic proteins in fracture repair, *International Orthopaedics*, 2018, **42**, 2619-2626, doi: 10.1007/s00264-018-4153-y.

[7] C. D. Lopez, J. M. Bekisz, C. Corciulo, A. Mediero, P. G.

Coelho, L. Witek, R. L. Flores, B. N. Cronstein, Local delivery of adenosine receptor agonists to promote bone regeneration and defect healing, *Advanced Drug Delivery Reviews*, 2019, **146**, 240-247, doi: 10.1016/j.addr.2018.06.010.

[8] A. Mediero, T. Wilder, L. Shah, B. N. Cronstein, Adenosine A_{2A} receptor (A2AR) stimulation modulates expression of semaphorins 4D and 3A, regulators of bone homeostasis, *The FASEB Journal*, 2018, **32**, 3487-3501, doi: 10.1096/fj.201700217r.

[9] J. M. Chun, A. Y. Lee, B. C. Moon, G. Choi, J.-S. Kim, Effects of dipsacus asperoides and phlomis umbrosa extracts in a rat model of osteoarthritis, *Plants*, 2021, **10**, 2030, doi: 10.3390/plants10102030.

[10] B.-S. Kim, Y.-C. Kim, H. Zadeh, Y.-J. Park, P. I. Sung-Hee, H.-S. Shin, H.-K. You, Effects of the dichloromethane fraction of dipsaci radix on the osteoblastic differentiation of human alveolar bone marrow-derived mesenchymal stem cells, *Bioscience, Biotechnology, and Biochemistry*, 2011, **75**, 13-19, doi: 10.1271/bbb.100379.

[11] X. Sun, B. Wei, Z. Peng, Q. Fu, C. Wang, J. Zhen, J. Sun, Protective effects of Dipsacus asper polysaccharide on osteoporosis *in vivo* by regulating RANKL/RANK/OPG/VEGF and PI3K/Akt/eNOS pathway, *International Journal of Biological Macromolecules*, 2019, **129**, 579-587, doi: 10.1016/j.ijbiomac.2019.02.022.

[12] Y. Tao, L. Chen, J. Yan, Traditional uses, processing methods, phytochemistry, pharmacology and quality control of *Dipsacus asper* Wall. ex C.B. Clarke: a review, *Journal of Ethnopharmacology*, 2020, **258**, 112912, doi: 10.1016/j.jep.2020.112912.

[13] Y. Zhai, L. Liu, F. Zhang, X. Chen, H. Wang, J. Zhou, K. Chai, J. Liu, H. Lei, P. Lu, M. Guo, J. Guo, J. Wu, Network pharmacology: a crucial approach in traditional Chinese medicine research, *Chinese Medicine*, 2025, **20**, 8, doi: 10.1186/s13020-024-01056-z.

[14] S. Li, B. Zhang, Traditional Chinese medicine network pharmacology: theory, methodology and application, *Chinese Journal of Natural Medicines*, 2013, **11**, 110-120, doi: 10.1016/s1875-5364(13)60037-0.

[15] L. Zhao, H. Zhang, N. Li, J. Chen, H. Xu, Y. Wang, Q. Liang, Network pharmacology, a promising approach to reveal the pharmacology mechanism of Chinese medicine formula, *Journal of Ethnopharmacology*, 2023, **309**, 116306, doi: 10.1016/j.jep.2023.116306.

[16] D. Dong, Z. Xu, W. Zhong, S. Peng, Parallelization of molecular docking: a review, *Current Topics in Medicinal Chemistry*, 2018, **18**, 1015-1028, doi: 10.2174/1568026618666180821145215.

[17] A. Bisht, D. Tewari, S. Kumar, S. Chandra, Network pharmacology, molecular docking, and molecular dynamics simulation to elucidate the mechanism of anti-aging action of Tinospora cordifolia, *Molecular Diversity*, 2024, **28**, 1743-1763, doi: 10.1007/s11030-023-10684-w.

[18] X. Wang, C. Yan, T. Wang, Y. Li, Z. Zheng, Mechanisms of luteolin against gastro-esophageal reflux disease based on network pharmacology, molecular docking, and molecular dynamics simulation, *Cell Biochemistry and Biophysics*, 2025, **83**, 403-414, doi: 10.1007/s12013-024-01471-x.

[19] X. Zha, R. Ji, Y. Li, R. Cao, S. Zhou, Network pharmacology, molecular docking, and molecular dynamics simulation analysis reveal the molecular mechanism of halociline against gastric cancer, *Molecular Diversity*, 2025, **29**, 4693-4703, doi: 10.1007/s11030-024-10822-y.

[20] J. Ru, P. Li, J. Wang, W. Zhou, B. Li, C. Huang, P. Li, Z. Guo, W. Tao, Y. Yang, X. Xu, Y. Li, Y. Wang, L. Yang, TCMSP: a database of systems pharmacology for drug discovery from herbal medicines, *Journal of Cheminformatics*, 2014, **6**, 13, doi: 10.1186/1758-2946-6-13.

[21] H. Dashti, J. R. Wedell, W. M. Westler, J. L. Markley, H. R. Eghbalnia, Automated evaluation of consistency within the PubChem compound database, *Scientific Data*, 2019, **6**, 190023, doi: 10.1038/sdata.2019.23.

[22] A. Daina, O. Michielin, V. Zoete, SwissADME: a free web tool to evaluate pharmacokinetics, drug-likeness and medicinal chemistry friendliness of small molecules, *Scientific Reports*, 2017, **7**, 42717, doi: 10.1038/srep42717.

[23] A. Daina, O. Michielin, V. Zoete, SwissTargetPrediction: updated data and new features for efficient prediction of protein targets of small molecules, *Nucleic Acids Research*, 2019, **47**, W357-W364, doi: 10.1093/nar/gkz382.

[24] W. Zhong, S.-Y. Tao, X. Guo, X.-F. Cheng, Q. Yuan, C.-X. Li, H.-Y. Tian, S. Yang, D. Sunchuri, Z.-L. Guo, Network pharmacology and molecular docking-based investigation on traditional Chinese medicine Astragalus membranaceus in oral ulcer treatment, *Medicine*, 2023, **102**, e34744, doi: 10.1097/md.0000000000034744.

[25] J. S. Amberger, C. A. Bocchini, F. Schiettecatte, A. F. Scott, A. Hamosh, OMIM.org: Online Mendelian Inheritance in Man (OMIM®), an online catalog of human genes and genetic disorders, *Nucleic Acids Research*, 2015, **43**, D789-D798, doi: 10.1093/nar/gku1205.

[26] C. Knox, M. Wilson, C. M. Klinger, M. Franklin, E. Oler, A. Wilson, A. Pon, J. Cox, N. E. Chin, S. A. Strawbridge, M. Garcia-Patino, R. Kruger, A. Sivakumaran, S. Sanford, R. Doshi, N. Khetarpal, O. Fatokun, D. Doucet, A. Zubkowski, D. Y. Rayat, H. Jackson, K. Harford, A. Anjum, M. Zakir, F. Wang, S. Tian, B. Lee, J. Liigand, H. Peters, R. Q. Wang, T. Nguyen, D. So, M. Sharp, R. da Silva, C. Gabriel, J. Scantlebury, M. Jasinski, D.

Ackerman, T. Jewison, T. Sajed, V. Gautam, D. S. Wishart, DrugBank 6.0: the DrugBank knowledgebase, *Nucleic Acids Research*, 2024, **52**, D1265-D1275, doi: 10.1093/nar/gkad976.

[27] T. U. Consortium, A. Bateman, M.-J. Martin, S. Orchard, M. Magrane, S. Ahmad, E. Alpi, E. H. Bowler-Barnett, R. Britto, H. Bye-A-Jee, A. Cukura, P. Denny, T. Dogan, T. Ebenezer, J. Fan, P. Garmiri, L. J. da Costa Gonzales, E. Hatton-Ellis, A. Hussein, A. Ignatchenko, G. Insana, R. Ishtiaq, V. Joshi, D. Jyothi, S. Kandasaamy, A. Lock, A. Luciani, M. Lugaric, J. Luo, Y. Lussi, A. MacDougall, F. Madeira, M. Mahmoudy, A. Mishra, K. Moulang, A. Nightingale, S. Pundir, G. Qi, S. Raj, P. Raposo, D. L. Rice, R. Saidi, R. Santos, E. Speretta, J. Stephenson, P. Totoo, E. Turner, N. Tyagi, P. Vasudev, K. Warner, X. Watkins, R. Zaru, H. Zellner, A. J. Bridge, L. Aimo, G. Argoud-Puy, A. H. Auchincloss, K. B. Axelsen, P. Bansal, D. Baratin, T. M. Batista Neto, M.-C. Blatter, J. T. Bolleman, E. Boutet, L. Breuza, B. C. Gil, C. Casals-Casas, K. C. Echioukh, E. Coudert, B. Cuche, E. de Castro, A. Estreicher, M. L. Famiglietti, M. Feuermann, E. Gasteiger, P. Gaudet, S. Gehant, V. Gerritsen, A. Gos, N. Gruaz, C. Hulo, N. Hyka-Nouspikel, F. Jungo, A. Kerhornou, P. Le Mercier, D. Lieberherr, P. Masson, A. Morgat, V. Muthukrishnan, S. Paesano, I. Pedruzzi, S. Pilbout, L. Pourcel, S. Poux, M. Pozzato, M. Pruess, N. Redaschi, C. Rivoire, C. J. A. Sigrist, K. Sonesson, S. Sundaram, C. H. Wu, C. N. Arighi, L. Arminski, C. Chen, Y. Chen, H. Huang, K. Laiho, P. McGarvey, D. A. Natale, K. Ross, C. R. Vinayaka, Q. Wang, Y. Wang, J. Zhang, UniProt: the universal protein knowledgebase, *Nucleic Acids Research*, 2023, **51**, D523-D531, doi: 10.1093/nar/gkac1052.

[28] D. Szklarczyk, R. Kirsch, M. Koutrouli, K. Nastou, F. Mehryary, R. Hachilif, A. L. Gable, T. Fang, N. T. Doncheva, S. Pyysalo, P. Bork, L. J. Jensen, C. von Mering, The STRING database in 2023: protein–protein association networks and functional enrichment analyses for any sequenced genome of interestOpen access, *Nucleic Acids Research*, 2023, **51**, D638-D646, doi: 10.1093/nar/gkac1000.

[29] D. Otasek, J. H. Morris, J. Bouças, A. R. Pico, B. Demchak, Cytoscape Automation: empowering workflow-based network analysis, *Genome Biology*, 2019, **20**, 185, doi: 10.1186/s13059-019-1758-4.

[30] C.-H. Chin, S.-H. Chen, H.-H. Wu, C.-W. Ho, M.-T. Ko, C.-Y. Lin, cytoHubba: identifying hub objects and sub-networks from complex interactome, *BMC Systems Biology*, 2014, **8**, doi: 10.1186/1752-0509-8-S4-S11.

[31] Y. Zhou, B. Zhou, L. Pache, M. Chang, A. H. Khodabakhshi, O. Tanaseichuk, C. Benner, S. K. Chanda, Metascape provides a biologist-oriented resource for the analysis of systems-level datasets, *Nature Communications*, 2019, **10**, 1523, doi: 10.1038/s41467-019-09234-6.

[32] A. S. Rose, A. R. Bradley, Y. Valasatava, J. M. Duarte, A. Prlić, P. W. Rose, NGL viewer: web-based molecular graphics for large complexes, *Bioinformatics*, 2018, **34**, 3755-3758, doi: 10.1093/bioinformatics/bty419.

[33] N. M. O'Boyle, M. Banck, C. A. James, C. Morley, T. Vandermeersch, G. R. Hutchison, Open Babel: an open chemical toolbox, *Journal of Cheminformatics*, 2011, **3**, doi: 10.1186/1758-2946-3-33.

[34] Y. Zhang, M. F. Sanner, *AutoDock CrankPep*: combining folding and docking to predict protein–peptide complexes, *Bioinformatics*, 2019, **35**, 5121-5127, doi: 10.1093/bioinformatics/btz459.

[35] G. M. Morris, R. Huey, W. Lindstrom, M. F. Sanner, R. K. Belew, D. S. Goodsell, A. J. Olson, AutoDock4 and AutoDockTools4: Automated docking with selective receptor flexibility, *Journal of Computational Chemistry*, 2009, **30**, 2785-2791, doi: 10.1002/jcc.21256.

[36] B. H. M. Mooers, M. E. Brown, Templates for writing PyMOL scripts, *Protein Science*, 2021, **30**, 262-269, doi: 10.1002/pro.3997.

[37] C. I. Bayly, P. Cieplak, W. Cornell, P. A. Kollman, A well-behaved electrostatic potential based method using charge restraints for deriving atomic charges: the RESP model, *The Journal of Physical Chemistry*, 1993, **97**, 10269-10280, doi: 10.1021/j100142a004.

[38] M. J. Abraham, T. Murtola, R. Schulz, S. Páll, J. C. Smith, B. Hess, E. Lindahl, GROMACS: High performance molecular simulations through multi-level parallelism from laptops to supercomputers, *SoftwareX*, 2015, **1-2**, 19-25, doi: 10.1016/j.softx.2015.06.001.

[39] K.-Y. Hsin, S. Ghosh, H. Kitano, Combining machine learning systems and multiple docking simulation packages to improve docking prediction reliability for network pharmacology, *PLoS One*, 2013, **8**, e83922, doi: 10.1371/journal.pone.0083922.

[40] A. N. Kristanti, N. S. Aminaha, I. Siswanto, A. P. Wardana, M. I. Abdjan, A. R. Khoirunisak, E. Noviana, Synthesis, pharmacokinetic, molecular docking, and molecular dynamics simulation of 2-styrylchromone derivatives as potential inhibitor of human kinesin Eg5, *Engineered Science*, 2024, **30**, 1168, doi: 10.30919/es1168.

[41] J. Gao, L. Yuan, H. Jiang, G. Li, Y. Zhang, R. Zhou, W. Xian, Y. Zou, Q. Du, X. Zhou, Naringenin modulates oxidative stress and lipid metabolism: Insights from network pharmacology, mendelian randomization, and molecular docking, *Frontiers in Pharmacology*, 2024, **15**, 1448308, doi: 10.3389/fphar.2024.1448308.

[42] H. Zhang, L. Liu, C. Jiang, K. Pan, J. Deng, C. Wan, MMP9 protects against LPS-induced inflammation in osteoblasts, *Innate Immunity*, 2020, **26**, 259-269, doi: 10.1177/1753425919887236.

[43] M. P. Whyte, Carbonic anhydrase II deficiency, *Bone*, 2023,

169, 116684, doi: 10.1016/j.bone.2023.116684.